Formaldehyde production from isoprene oxidation across NO_x regimes

G. M. Wolfe[1,2], J. Kaiser[3], T. F. Hanisco[2], F. N. Keutsch[4], J. A. de Gouw[5,6], J. B. Gilman[5,6], M. Graus[5,6,*], C. D. Hatch[7], J. Holloway[5,6], L. W. Horowitz[9], B. H. Lee[8], B. M. Lerner[5,6], F. Lopez-Hilifiker[8], J. Mao[9,11], M. Marvin[10], J. Peischl[5,6], I. B. Pollack[5,6], J. M. Roberts[6], T. B. Ryerson[6], J. A. Thornton[8], P. R. Veres[5,6], C. Warneke[5,6]

[1]Joint Center for Earth Systems Technology, University of Maryland Baltimore County, Baltimore, MD, USA

[2]Atmospheric Chemistry and Dynamics Laboratory, NASA Goddard Space Flight Center, Greenbelt, MD, USA

[3]Department of Chemistry, University of Wisconsin-Madison, Madison, WI, USA

[4]School of Engineering and Applied Sciences and Department of Chemistry and Chemical Biology, Harvard University, Cambridge, MA, USA

[5]Cooperative Institute for Research in Environmental Sciences, University of Colorado Boulder, Boulder, CO, USA

[6]Chemical Sciences Division, NOAA Earth System Research Laboratory, Boulder, CO, USA

[7]Department of Chemistry, Hendrix College, Conway, AR, USA

[8]Department of Atmospheric Sciences, University of Washington, Seattle, WA, USA

[9]NOAA Geophysical Fluid Dynamics Laboratory, Princeton, NJ, USA

[10]Department of Chemistry, University of Maryland, College Park, MD, USA

[11]Program in Atmospheric and Oceanic Sciences, Princeton University, Princeton, NJ

*Now at Institute of Atmospheric and Cryospheric Sciences, Innsbruck University, Austria

Correspondence to G. M. Wolfe (glenn.m.wolfe@nasa.gov)

Abstract

The chemical link between isoprene and formaldehyde (HCHO) is a strong, non-linear function of NO_x (= NO + NO_2). This relationship is a linchpin for top-down isoprene emission inventory verification from orbital HCHO column observations. It is also a benchmark for overall mechanism performance with regard to VOC oxidation. Using a comprehensive suite of airborne *in situ* observations over the Southeast U.S., we quantify HCHO production across the urban-rural spectrum. Analysis of isoprene and its major first-generation oxidation products allows us to define both a "prompt" yield of HCHO (molecules of HCHO produced per molecule of freshly-emitted isoprene) and the background HCHO mixing ratio (from oxidation of longer-lived hydrocarbons). Over the range of observed NO_x values (roughly 0.1 – 2 ppbv), the prompt yield increases by a factor of 3 (from 0.3 to 0.9), while background HCHO increases by more than a factor of 2 (from 1.5 to 3.3 ppbv). We apply the same method to evaluate the performance of both a global chemical transport model (AM3) and a measurement-constrained 0-D chemical box model. Both models reproduce the NO_x dependence of the prompt HCHO yield, illustrating that models with updated isoprene oxidation mechanisms can adequately capture the link between HCHO and recent isoprene emissions. On the other hand, both models under-estimate background HCHO mixing ratios, suggesting missing HCHO precursors, inadequate representation of later-generation isoprene degradation and/or under-estimated hydroxyl radical concentrations. Moreover, we find that the total organic peroxy radical production rate is essentially independent of NO_x, as the increase in oxidizing capacity with NO_x is largely balanced by a decrease in VOC reactivity. Thus, the observed NO_x dependence of HCHO mainly reflects the changing fate of organic peroxy radicals.

1. Introduction

Formaldehyde (HCHO) is a ubiquitous byproduct of volatile organic compound (VOC) oxidation. While methane is the principal HCHO precursor in remote regions, larger VOC are the main source over continents. HCHO is also directly emitted via biomass burning (Lee et al., 1997), fossil fuel combustion (Luecken et al., 2012), natural gas flaring (Knighton et al., 2012), ethanol refining (de Gouw et al., 2015), possibly vegetation (DiGangi et al., 2011) and agricultural activity (Kaiser et al., 2015a), but chemical production dominates the global budget (Fortems-Cheiney et al., 2012). Photolysis and reaction with OH

destroy HCHO with a characteristic lifetime of several hours during midday, implying that the HCHO abundance reflects recent hydrocarbon oxidation.

Globally, isoprene is the main precursor of near-surface HCHO. A highly reactive diene emitted by vegetation, isoprene comprises roughly one third of all non-methane VOC emissions (Guenther et al., 2012). Oxidation of isoprene in the presence of nitrogen oxides (NO_x = NO + NO_2) stimulates the production of ozone (Trainer et al., 1987) and organic aerosol precursors (Xu et al., 2015), impacting air quality and climate in many continental regions. Despite the central role of isoprene, biogenic emission inventories struggle to accurately represent the spatiotemporal variability of isoprene emissions, with model-measurement discrepancies and differences among emission inventories approaching a factor of 2 or more (Carlton and Baker, 2011; Warneke et al., 2010). Such differences directly impact predicted ozone and aerosol distributions (Hogrefe et al., 2011).

Numerous studies have applied satellite-based HCHO column observations as a top-down constraint on isoprene emissions (see Kefauver et al. (2014) for a review). Typically, a chemical transport model is employed to relate HCHO column concentrations to isoprene emission strength. Early studies utilized linear steady-state relationships (Palmer et al., 2003), while recent computational advances have permitted full inversions that more fully account for transport, multiple sources and varying chemical regimes (Fortems-Cheiney et al., 2012). Such techniques have informed isoprene emission inventories in North America (Abbot et al., 2003; Millet et al., 2008; Millet et al., 2006; Palmer et al., 2006; Palmer et al., 2003), South America (Barkley et al., 2013; Barkley et al., 2008), Europe (Curci et al., 2010; Dufour et al., 2009), Africa (Marais et al., 2012), Asia (Fu et al., 2007; Stavrakou et al., 2014), and globally (Fortems-Cheiney et al., 2012; Shim et al., 2005; Stavrakou et al., 2009). Future geostationary observations, such as the NASA Tropospheric Emissions: Monitoring of Pollution (TEMPO, http://science.nasa.gov/missions/tempo/) mission, will permit an even more detailed investigation of the spatial and temporal variability of isoprene emissions and other VOC sources.

Chemistry dictates the relationship between HCHO columns and underlying isoprene emissions. Many of the above-listed studies apply 0-D box model calculations to evaluate the yield of HCHO from isoprene as a function of oxidation time, NO_x regime and chemical mechanism. In all cases, it is found that NO_x enhances both the production rate and ultimate yield of HCHO. Slower production at lower NO_x can lead to "smearing," whereby HCHO production is displaced relative to the isoprene source. Palmer et al. (2003) define a characteristic smearing length scale, which can range from 10 to 100 km or more. Furthermore, accumulation of oxygenated VOC over multiple generations of isoprene

degradation can contribute to substantial background HCHO production, which is not directly linked with fresh isoprene emissions. Long-lived primary anthropogenic or biogenic emissions, like methane and methanol, can also contribute to this background. Background column concentrations are typically on the order of 5×10^{15} cm^{-2}, equating to 20% or more of the isoprene-driven HCHO column enhancement (Barkley et al., 2013; Millet et al., 2006). A wave of recent theoretical (Peeters et al., 2014; Peeters and Müller, 2010; Peeters et al., 1999), laboratory (Crounse et al., 2012; Crounse et al., 2011; Paulot et al., 2009a; Paulot et al., 2009b) and field (Mao et al., 2012) research has highlighted shortcomings in low-NO_x isoprene oxidation schemes. Such issues translate directly into top-down emission estimates; for example, Marais et al. (2012) report an uncertainty of 40% in OMI-derived African isoprene emissions at high-NO_x and 40-90% at low-NO_x. Coarse resolution of averaged satellite observations and model simulations (typically $1° \times 1°$ or more) has partly mitigated these problems in prior work, as variability in NO_x-dependent smearing and background production is averaged out. A more careful treatment will be needed to harness the enhanced resolution of near-future orbital observations (e.g., 8×4.5 km^2 for TEMPO), especially since these measurements will include diurnal variability.

Here, we use a comprehensive set of *in situ* observations to quantify the impact of NO_x on the isoprene-HCHO chemical link. Using isoprene and its unique first-generation products, we segregate HCHO into two categories. The first, defined as "prompt" HCHO, is produced from fresh isoprene emissions (on a timescale of less than a day) and retains the signature of isoprene emission source strength. The second category is "background" HCHO stemming from oxidation of longer-lived isoprene oxidation products and other VOC. We examine the NO_x dependence of both quantities. Applying the same method to 0-D and global model simulations, we evaluate the ability of current chemical mechanisms to replicate the observed trends. Box model results are also used to elucidate the mechanistic underpinnings of the NO_x influence on HCHO production.

2. SENEX Observations

The Southeast Nexus (SENEX) mission was an airborne campaign designed to examine the interaction of natural and anthropogenic emissions. During June and July of 2013, the NOAA WP-3D aircraft logged 114 flight hours over 18 research flights in a range of environments throughout the southeast United States, including urban centers, power plant plumes, natural gas extraction regions, agricultural areas

and forests. The payload included a suite of gas- and particle-phase instrumentation (Warneke et al*., in preparation*, 2015); details and data are accessible on the SENEX website (http://www.esrl.noaa.gov/csd/projects/senex/). Here we utilize observations of HCHO, isoprene, methyl vinyl ketone (MVK), methacrolein (MACR), NO and NO_2. HCHO was measured at 1 Hz by the NASA In Situ Airborne Formaldehyde (ISAF) instrument, which relies on the laser-induced fluorescence technique and has an accuracy of ±10% (Cazorla et al., 2015). Isoprene, MVK and MACR were measured by both a quadrupole proton transfer reaction mass spectrometer (PTR-MS) and the NOAA improved whole-air sampler (iWAS) with offline gas chromatography. The PTR-MS (de Gouw and Warneke, 2007) has a stated accuracy of 20% and sequentially sampled masses for isoprene (m/z +69) and the sum of MVK and MACR (m/z +71) for 1 s each with a duty cycle of 14 s. The iWAS measurement uncertainty for speciated MVK and MACR is 20% (de Gouw et al., 2015). NO and NO_2 were measured at 1 Hz via chemiluminescence coupled with a photolytic NO_2 converter (Pollack et al., 2010; Ryerson et al., 1999) with an accuracy of 5%. Data are filtered to include only daytime boundary layer conditions (solar zenith angle < 60°, radar altitude < 1 km). Influence from biomass burning (acetonitrile > 210 pptv and CO > 300 ppbv) and very fresh power plant plumes ($\log(NO_x)$ values exceeding a mean + 3σ threshold) are also removed. This procedure excludes 50% of all fast (1 Hz) data. After accounting for missing data, we retain 8435 1 Hz data points and 81 iWAS samples.

Measurements of MVK and MACR can include a positive bias from conversion of isoprene hydroxyhydroperoxides (ISOPOOH) on hot metal surfaces in the sampling system (Liu et al., 2013; Rivera-Rios et al., 2014). Theoretically, this mechanism could give rise to an analogous artifact in HCHO observations. ISOPOOH mixing ratios of roughly 0 to 2 ppbv were observed during SENEX (see supporting information (SI)). It is difficult to quantify the magnitude of any such interference from field observations alone. Based on a comparison to observations of other isoprene oxidation products and to 0-D box model results (SI), we argue that such artifacts are negligibly small in the PTR-MS and ISAF observations for SENEX. We cannot rule out a potential positive bias in the iWAS MVK measurement; nonetheless, as we show below, the correspondence between observed MVK and MACR mixing ratios is consistent with our current understanding of isoprene oxidation.

SENEX sampled a wide spectrum of chemical regimes (Figure 1). For the daytime boundary-layer observations presented here, maximum 1 Hz isoprene and NO mixing ratios respectively reach 8.1 and 95 ppbv, while minima are less than a few pptv. The distributions of both isoprene and NO observations are approximately log-normal (top and right panels of Fig. 1), peaking at 1.5 ppbv and 50 pptv,

147 respectively. Though these distributions may be biased towards areas of urban influence, the range of
148 environments encountered during SENEX is representative of the Southeast U.S. summertime boundary
149 layer. The long tail at the low end of the isoprene distribution is mostly associated with regions lacking
150 significant tree cover, notably Illinois and Indiana, where isoprene emissions are generally lower. The NO
151 distribution spans two orders of magnitude (10 – 1000 pptv), over which radical chemistry changes
152 markedly. At NO mixing ratios of a few hundred pptv or more, organic peroxy radicals (RO_2) react mostly
153 with NO. At low NO (10's of pptv or less), reaction with HO_2, other RO_2 and isomerization dominate. The
154 bulk of the NO_x distribution lies in a transition region for radical chemistry, making this dataset ideal for
155 probing the anthropogenic influence on biogenic VOC oxidation.

156 HCHO mixing ratios (color shading in Fig. 1) range from 0.8 to 14 ppbv with a mean value of 4.3
157 ppbv. HCHO is most abundant in regions where both isoprene and NO_x are elevated. High NO_x is often
158 accompanied by increased concentrations of anthropogenic VOC; however, constrained box-model
159 calculations demonstrate that isoprene is the dominant HCHO precursor even in these cases (Sect. 5).
160 Thus, chemistry (and not co-variance of NO_x and anthropogenic VOC) drives the observed NO_x
161 dependence of HCHO abundance.

162

163 **3. Linking Observed and Emitted Isoprene**

164 The isoprene photochemical cascade is a multi-step process. Isoprene oxidation is initiated by reaction
165 with the hydroxyl radical (OH), ozone or the nitrate radical (NO_3). In the Southeast U.S., typical daytime
166 levels for OH, ozone and NO_3 are 4×10^6 cm^{-3}, 50 ppbv and 0.1 pptv, respectively (OH and NO_3 are
167 estimated from median box model output, see Sect. 5). The corresponding isoprene lifetimes at 298K
168 are 0.7 h, 17 h and 160 h, respectively. Thus, reaction with OH typically constitutes 95% or more of the
169 total daytime isoprene sink in this environment. Addition of OH and reaction with O_2 generates one of
170 several isoprene hydroxyperoxy radicals ($ISOPO_2$). $ISOPO_2$ isomers interconvert rapidly due to reversible
171 O_2 addition (Peeters et al., 2009) but are eventually destroyed via reaction with NO, hydroperoxy radical
172 (HO_2), other organic peroxy radicals (RO_2) or isomerization. Most branches have the potential to
173 produce HCHO, with varying yields. The laboratory-derived first-generation HCHO yield from the NO
174 pathway is ~0.6 (Atkinson and Arey, 2003), though this value may be less representative of the real
175 atmosphere due to the very high isoprene concentrations (and very short RO_2 lifetimes) in early
176 chamber experiments. The first-generation yield from the HO_2 pathway is ~0.06 (Liu et al., 2013).

Isomerization chemistry is less well understood; the 1,5-H-shift is believed to produce HCHO with a unity yield, while the much faster 1,6-H-shift should not produce any HCHO (da Silva et al., 2010; Fuchs et al., 2013; Peeters et al., 2014; Peeters and Müller, 2010; Peeters et al., 2009). Regardless of the specific pathway, MVK or MACR are always co-produced with HCHO in the first generation. HCHO is also generated in subsequent chemistry, but on a longer timescale and from a much larger suite of precursors. For example, the OH lifetimes of MACR and MVK are respectively 3.5 and 5 times longer than that of isoprene.

Boundary layer composition reflects a mixture of emissions with various degrees of photochemical processing. To isolate the impact of "fresh" isoprene emissions, we exploit the relatively simple chemistry of MVK and MACR, which are produced via isoprene oxidation and lost primarily via reaction with OH.

$$\text{ISOP} + \text{OH} \rightarrow y_{MACR}\text{MACR} + y_{MVK}\text{MVK} \qquad k_1 = 2.7\times10^{-11}\, e^{390/T} \qquad \text{(R1)}$$

$$\text{MACR} + \text{OH} \rightarrow \text{products} \qquad k_2 = 8.0\times10^{-12}\, e^{380/T} \qquad \text{(R2)}$$

$$\text{MVK} + \text{OH} \rightarrow \text{products} \qquad k_3 = 2.6\times10^{-12}\, e^{610/T} \qquad \text{(R3)}$$

Rate constants (*k*) are taken from the IUPAC database (Atkinson et al., 2006). These reactions form the basis for a photochemical clock of isoprene oxidation (de Gouw et al., 2005; Roberts et al., 2006; Stroud et al., 2001). Integration of the kinetic equations for this system shows that the product/parent ratios are a function of the rate constants, yield (*y*), reaction time (*t*) and the mean OH concentration averaged over reaction time. In the case of MACR, for example:

$$\frac{[MACR]}{[ISOP]} = \frac{y_{MACR}k_1}{k_2-k_1}\left(1 - e^{(k_1-k_2)[OH]t}\right) \qquad (1)$$

An analogous expression holds for MVK. As noted by Stroud et al. (2001), this "sequential reaction model" is purely chemical and does not account for the effects of mixing and transport. Indeed, this analysis relates daughter/parent ratios to an "average" photochemical age, when in fact there is a broad distribution of ages in any mixed air mass. We also implicitly assume that direct emissions (Fares et al., 2015) and deposition (Karl et al., 2010) of MVK and MACR do not significantly influence the budget of these compounds.

Two potential issues arise when applying this model to the real atmosphere. First, the yields of MVK and MACR are dependent on $ISOPO_2$ branching and are thus a non-linear function of NO_x. Previous

applications of this method (de Gouw et al., 2005; Roberts et al., 2006; Stroud et al., 2001) have assumed lab-derived high-NO_x yields of 0.33 and 0.23 for MVK and MACR, respectively (Atkinson and Arey, 2003), but this may not be appropriate in the present case; furthermore, these yields are not fully consistent with current chemical mechanisms (Fig. S4). We explicitly examine the effects of NO_x-varying yields below using yield curves derived from box model simulations (see SI for details). Second, the photochemical age (*t*) implied by any observed daughter/parent ratio depends on the concentration of OH, which was not measured and varies as an air mass ages. Rather than assume a single "typical" value for OH, we express photochemical age in terms of "exposure," defined here as the product of OH concentration and reaction time integrated over the photochemical lifetime of an air mass.

Figure 2 compares the observed relationship of MVK/isoprene and MACR/isoprene ratios against theoretical trends predicted by the sequential reaction model. Theoretical ratios are calculated at fixed exposures of 2, 4, 8, 12 and 16$\times$ 10^6 OH cm^{-3} h using two sets of yields: high NO (NO = 1000 pptv, y_{MVK} = 0.41, y_{MACR} = 0.28) and low NO (NO = 50 pptv, y_{MVK} = 0.21, y_{MACR} = 0.19). Observed ratios of MVK/isoprene versus MACR/isoprene exhibit a tight linear correlation (Fig. 2). Higher ratios are often associated with higher NO_x, likely reflecting enhanced OH and higher HCHO yields in these air masses. Far downwind from isoprene and NO_x source regions, we would expect to see higher MVK/isoprene and MACR/isoprene ratios associated with lower NO_x due to removal of the latter. The theoretical slope agrees well with observations, indicating exposures of 1 – 16 $\times$ 10^6 OH cm^{-3} h. For a typical daytime OH concentration of 4 $\times$ 10^6 cm^{-3}, this corresponds to processing times of 15 minutes to 4 hours.

The ratio of y_{MVK} to y_{MACR} dictates the location of the theoretical line and thus the correspondence between daughter/parent ratios and exposure. For example, a MACR/isoprene ratio of 1 would be consistent with an exposure of 4.9 x 10^6 OH cm^{-3} h at high-NO_x conditions (NO = 1000 pptv) versus 6.1 x 10^6 OH cm^{-3} h at low-NO_x (NO = 50 pptv). Thus, for any given daughter/parent ratio, a higher assumed yield gives a smaller derived exposure. Observations in Fig. 2 fall above the high-NO_x theoretical relationship. As discussed in the SI, however, iWAS MVK measurement may contain a positive artifact on the order of 50%. This potential systematic error (thick black line in Fig. 2) overlaps both the high and low-NO_x theoretical relationships. Given the wide range of conditions sampled, it is most appropriate to use a NO_x-dependent yield for MVK and MACR. For this purpose, model-derived yields (Fig. S4 and SI) are interpolated to observed NO mixing ratios.

We can effectively reverse this photochemical clock to derive a proxy for the total isoprene emissions that had been released into the sample air masses (de Gouw et al., 2005). First, we calculate OH exposures from observed daughter/parent ratios by inverting Eqn. (1). To perform this calculation with PTR-MS data (which has far greater coverage), we partition the measured sum between MVK and MACR using MVK/MACR ratios from box model calculations (Sect. 5). Modeled MVK/MACR ratios (with an output interval of 1 minute) are linearly interpolated to the 14-second observational time base. The MVK/MACR ratio does not vary dramatically (mean ± 1σ: 1.3 ± 0.2), and using a constant ratio instead alters results by less than 4%. Calculated exposures range from 0.5 to 18 × 10^6 OH cm^{-3} h (Fig. S5A). Exposures derived from MACR are 6% higher than those from MVK on average, and we use the mean of these two values. Next, an "initial" isoprene mixing ratio, $ISOP_0$, is estimated via reverse integration of isoprene's first-order loss rate:

$$[ISOP]_0 = [ISOP]e^{k_1[OH]t} \quad (2)$$

$ISOP_0$ represents the amount of isoprene that an air parcel would have to start with to generate the amount of isoprene, MVK and MACR observed. Thus, it is an observationally-constrained surrogate for isoprene emission strength (modulated to some degree by boundary layer height, as it is a volume-based quantity). $ISOP_0$ mixing ratios are typically 2 – 10 times higher than observed isoprene (Fig. S5B).

4. The Yield of HCHO from Isoprene

The definition of "yield" can vary with context and requires careful consideration when quantifying the isoprene-HCHO relationship. In a mechanistic sense, the "first generation yield" refers to the amount of HCHO produced per unit isoprene consumed in the first stage of oxidation. This is analogous to the yields of MVK and MACR used in the above calculation of initial isoprene. The model-derived first-generation HCHO yield from isoprene varies by more than a factor of 2 over the range of chemical environments encountered during SENEX (Fig. S4). An alternative definition is that of the "total yield" (sometimes referred to as the "molar yield," e.g. Millet et al. (2006)), a time-dependent quantity that describes the total amount of HCHO produced over multiple generations of oxidation. The total yield is typically derived from model simulations and used to relate satellite HCHO column observations to isoprene emissions (Marais et al., 2012; Millet et al., 2006). Early studies acknowledged the NO_x dependence of the total yield (Millet et al., 2006; Palmer et al., 2003) and more recent work has

attempted to account for the dependence using NO_2 column observations (Marais et al., 2012). Here, we define the "prompt yield" as the change in observed HCHO per unit change in $ISOP_0$ ($y_p = \Delta HCHO/\Delta ISOP_0$). This is not the same as the first-generation yield, since y_p can include HCHO production and loss over several hours (depending on the photochemical exposure of an air mass). Nor is it the same as the total yield, which inherently does not account for HCHO loss as an air mass ages. The prompt yield is effectively a quantity that relates isoprene emission strength to observed HCHO abundance. As we will demonstrate, y_p is well-suited for segregating the various drivers of HCHO and for benchmarking model performance.

Figure 3A shows the relationship between calculated $ISOP_0$ and observed HCHO. The overall correlation is linear with a striking NO_x gradient. To quantify this NO_x dependence, we sort the data by $\log(NO_x)$, group it into 20 bins such that each bin contains the same number of points (N = 416), and perform a major-axis linear fit of HCHO versus $ISOP_0$ for each bin. Individual fits give r^2 values of 0.6-0.8, except for the highest NO_x bin (r^2 = 0.48) that contains some heavily-polluted air masses, such as downwind from power plants. Results are independent of the number of bins chosen or time resolution (e.g., 1-second versus 1-minute data).

The HCHO-$ISOP_0$ slope (Fig. 3B) represents the prompt yield. This yield varies by a factor of 3 over the range of observed NO_x, from 0.3 for NO_x mixing ratios of a few hundred pptv to 0.9 at NO_x > 1 ppbv. At low NO_x, y_p is comparable to the MCM-predicted direct first-generation yield of HCHO (0.3-0.4 at NO = 10-40 pptv, Fig. S4), while at high NO_x it is somewhat higher than the predicted first-generation yield (0.74 at NO = 1000 pptv). This likely reflects the inclusion of more than one generation of HCHO production at higher NO_x, where oxidation is more rapid (median exposures increase by 38% over the range of observed NO_x values). Most of this portion of the HCHO budget, however, stems from first-generation production.

The intercept (Fig. 3C) represents the abundance of "background" HCHO. This portion of the HCHO budget stems mainly from air that either has not encountered strong isoprene emissions or is so aged that most of the isoprene has reacted away and can no longer be linked to a specific source region. Some of this background may also stem from oxidation of long-lived primary emissions like methane or methanol. Box model calculations (Sect. 5) indicate average HCHO budget contributions of 0.3 ± 0.2 ppbv and 0.2 ± 0.1 ppbv from methane and methanol, respectively. Background HCHO also exhibits a marked NO_x dependence, increasing from 1.6 to 3.3 ppbv over the observed NO_x range. As with y_p, we

293 expect such behavior since NO_x regulates the fate of all organic peroxy radicals (see Sect. 6). Assuming a
294 1 km mixed layer depth (Wagner et al., 2015), the corresponding HCHO column density for this
295 background is 4 – 8 x 10^{15} cm^{-2}. This is comparable to the background reported by previous
296 investigations of satellite-derived HCHO columns (Barkley et al., 2013; Millet et al., 2006). None of these
297 studies explicitly account for the NO_x dependence of the background, though it can represent a
298 substantial fraction of the total HCHO column – maximum summertime HCHO columns over the
299 southeast U.S. are ~25 x 10^{15} cm^{-2} (Millet et al., 2008). Given the strong NO_x dependence of both y_p and
300 background HCHO, grouping HCHO column observations by NO_x (e.g. using simultaneous observations of
301 NO_2 columns (Marais et al., 2012) or model-derived NO_x) and performing an analysis similar to that
302 described here should provide a robust means of accounting for these influences.

303

304 **5. Model Evaluation**

305 To illustrate the utility of this analysis, we compare the observed HCHO-$ISOP_0$ relationship to results
306 from a global chemical-transport model and a 0-D box model. Goals?

307 The GFDL AM3 model is an atmospheric general circulation model with interactive chemistry
308 (Donner et al., 2011), including recent updates to the representation of isoprene degradation (Mao et
309 al., 2013; Naik et al., 2013). Model simulations were carried out at 50 × 50 km^2 resolution with
310 horizontal winds nudged to NCEP GFS analyses and sampled along the SENEX flight tracks at a time
311 resolution of 1 minute. Further details are available elsewhere (Li et al., 2015).

312 The University of Washington Chemical Box Model (UWCM v2.2) is a versatile 0-dimensional
313 framework for simulating various chemical systems, including lab chamber experiments (Wolfe et al.,
314 2012) and observations from ground (Kim et al., 2015; Kim et al., 2013; Wolfe et al., 2014) and airborne
315 (Marvin et al., 2015) platforms. Multiple chemical mechanisms are available within UWCM; here we use
316 the latest version of the Master Chemical Mechanism (MCM v3.3, Jenkin et al. (2015)). UWCM is
317 constrained with 1-minute average observations of isoprene, NO_2, ozone, CO, PAN, methane, methanol
318 and meteorology and assumes clear-sky conditions for photolysis frequencies. The chemical system is
319 integrated forward in time to diel steady state (total integration time of 3 days) for each set of
320 measurements. This setup inherently assumes that the atmosphere is in chemical steady state – that is,
321 that production and loss of HCHO, MVK, MACR and other species are roughly balanced. This assumption
322 is rarely strictly true and may fail for highly-aged air masses (where isoprene is depleted) or close to

strong local emissions. Nonetheless, it is a fair approximation for the daytime well-mixed boundary layer observations that prevailed during SENEX. Monoterpenes and anthropogenic VOC are excluded from the simulation since observations of these species (from the iWAS) are relatively sparse. Separate sensitivity simulations utilizing the iWAS data suggest that observed monoterpenes and anthropogenic VOC (a subset of alkanes, alkenes and aromatics) increase modeled HCHO by 1 ± 2 % and 2 ± 3 %, respectively. A more detailed evaluation of box model performance is forthcoming (Marvin et al., 2015).

Output from both models is filtered for daytime, boundary-layer, non-biomass burning points using the same criteria as that for observations (Sect. 2). Both models adequately reproduce observed HCHO mixing ratios (Fig. S6). We perform the same analyses as described above to derive model y_p and background HCHO. Because of the reduced time resolution, we group results into 10 NO_x bins, instead of 20, before fitting. For AM3, this results in 172 points per bin and typical r^2 values of 0.5 – 0.8. For UWCM, there are 157 points per bin and all r^2 values are > 0.9.

Both AM3 and UWCM reproduce the observed NO_x dependence of the prompt yield (Fig. 4A). AM3 agrees well with observations in both magnitude and trend, though with some scatter at mid-NO_x levels. UWCM tends be slightly high throughout the whole NO_x range, which may reflect an over-estimation of first-generation HCHO production due to holding isoprene constant throughout the model step and/or assuming diel steady state. Regardless, these results suggest that both models provide excellent representation of early generation isoprene oxidation across NO_x regimes.

Background HCHO mixing ratios are under-predicted by 0.5 – 1 ppbv by both models (Fig. 4B). The range of under-prediction is consistent with the offsets between observed and modeled total HCHO abundances (Fig. S6 fit x-intercepts: 0.3 ppbv (AM3) and 0.9 ppbv (UWCM)). It is possible that both models are missing some HCHO precursors (e.g. from multi-generation isoprene oxidation or other VOC not related to isoprene). This is especially plausible for the UWCM simulation, which only includes isoprene, methane and methanol as primary VOC and does not account for horizontal transport. Under-estimated OH concentrations might also explain part of this discrepancy, though we cannot easily evaluate this possibility. AM3 performs somewhat better than UWCM in terms of overall magnitude but exhibits a less clear NO_x trend, which may reflect dilution over fairly large grid scales (note that the range of binned NO_x values is smaller for AM3 than both observations and the UWCM). This result again highlights the need to consider this background before using a model to interpret observed HCHO columns that effectively integrate HCHO sources over space and time.

6. Mechanistic Drivers of the NO_x – HCHO Relationship

Despite the complexity of gas-phase organic chemistry, the impact of NO_x on HCHO production essentially reduces to two factors: radical cycling and RO_2 branching. Increasing NO enhances the conversion of HO_2 to OH (R4) and thus accelerates VOC oxidation (R5) and HCHO loss. Subsequent production of HCHO depends on the structure and fate of RO_2 intermediates, which can react with NO, HO_2, other RO_2, or isomerize (R6).

$$NO + HO_2 \rightarrow NO_2 + OH \quad \text{(R4)}$$

$$VOC + OH \rightarrow RO_2 \quad \text{(R5)}$$

$$RO_2 + (NO, HO_2, RO_2, \text{isomerization}) \rightarrow \alpha HCHO \quad \text{(R6)}$$

Here, α represents a bulk branching ratio for HCHO production weighted over all RO_2 reactions. The RO_2 lifetime is typically less than 100 s during the day, so (R5) is the rate-limiting step in HCHO formation. The HCHO production rate is then equal to the product of the total RO_2 production rate and the bulk branching ratio.

To disentangle these factors, we extract chemical rates from the diel steady-state UWCM simulations discussed in Sect. 5. Figure 5 shows the gross production rates of total peroxy radicals and HCHO as a function of NO_x. Consistent with our earlier discussion, total HCHO production increases by more than a factor of 3 from low to high NO_x. In contrast, RO_2 production is effectively constant within model variability. Closer investigation (results not shown) reveals that a factor of 3 – 4 increase in OH concentrations between low and high NO_x is more than offset by a similar reduction in isoprene. The ratio of HCHO to RO_2 production rates gives an estimate for α, which increases from 0.14 to 0.39 across this NO_x range (Fig. 5). Though the total RO_2 production rate includes reactions that do not make HCHO, α is still a useful metric for the relationship between HCHO production and overall VOC oxidation. Based on this analysis, we conclude that changes in RO_2 branching are the dominant factor driving the NO_x dependence of HCHO production and abundance.

Increased OH also reduces the lifetime of HCHO, which may affect the HCHO budget if this reaction becomes competitive with photolysis. UWCM predicts an average HCHO photolysis lifetime of 4 hours and OH reaction lifetimes that range from 3 hours at high NO_x to 12 hours at low NO_x. Thus,

381 photolysis is typically the dominant loss process and the scaling of HCHO lifetime with OH is typically
382 weak. As a result, the net chemical tendency of HCHO (production minus loss, not shown) is positive and
383 increasing throughout the range of model NO_x conditions. Faster loss due to reaction with OH therefore
384 only slightly dampens the enhancement in HCHO production.

385

386 **7. Conclusions**

387 Using SENEX aircraft observations, we have quantified the NO_x dependence of the relationship between
388 isoprene emission strength and HCHO mixing ratios. Simultaneous measurements of isoprene, MVK and
389 MACR define a photochemical clock for isoprene oxidation, allowing separation of prompt HCHO
390 production (which retains the isoprene source signature) and background HCHO from late-generation
391 isoprene oxidation products, methane and other long-lived VOC. The prompt HCHO yield increases by a
392 factor of 3 (0.3 to 0.9 mol/mol) and the average background HCHO mixing ratio more than doubles (1.6
393 to 3.3 ppbv) over the range of NO_x values encountered in the southeast U.S. This analytical method is
394 applied to evaluate the performance of a global chemical transport model and a 0-D box model. Both
395 models accurately reproduce the observed NO_x trend of the prompt HCHO yield, indicating that both
396 chemical mechanisms accurately capture early-stage isoprene oxidation. On the other hand, both
397 models also under-predict background HCHO abundance by 0.5 – 1 ppbv, which may be a significant
398 fraction of total HCHO in some cases. This may suggest insufficient build-up of isoprene-derived long-
399 lived precursors in the models, missing VOC not related to isoprene, or insufficient OH. Box model
400 results also provide insight into the mechanistic drivers of the observed NO_x trends. We find that
401 increasing NO_x does not significantly affect total RO_2 production due to the cancelling effects of higher
402 OH and lower VOC, and thus the positive correlation between NO_x and HCHO primarily reflects the
403 changing fate of RO_2 radicals.

404 To our knowledge, there are no direct laboratory measurements of HCHO yields from low-NO_x
405 isoprene chemistry; thus, the results presented here constitute the first measurement-constrained
406 evaluation of the isoprene-HCHO link across NO_x regimes. The AM3 and MCMv3.3 mechanisms differ
407 substantially (the former is highly condensed while the latter is explicit), but both contain recent
408 updates to isoprene degradation. We expect that other mechanisms will also perform well if they
409 accurately reflect our current best understanding. The observations presented here do not include the
410 extremely-low NO_x regime (NO_x < 0.1 ppbv) typical of remote regions like the Amazon and equatorial

Africa. In such pristine regions, smearing of HCHO production is expected to be more severe (Barkley et al., 2013), and total HCHO production may be significantly lower if the RO_2 fate favors functionalization over fragmentation (e.g. isomerization). More work is needed to map out this area of the urban-rural spectrum. It may also be possible to apply the methods developed here to evaluate the chemistry of glyoxal, another key tracer of VOC oxidation that is also amenable to orbital observations (Kaiser et al., 2015b; Li et al., 2015) and is believed to be an important precursor for SOA (McNeill et al., 2012).

These results also carry implications for top-down isoprene emission estimates. Uncertainties in low-NO_x chemistry are often cited as the largest source of potential error in derived emissions (Marais et al., 2012; Palmer et al., 2006). Based on our analysis, current mechanisms appear to capture low-NO_x production of HCHO, MVK and MACR, thus such errors are likely less severe than commonly asserted. Recent work has acknowledged the impact of NO_x on the prompt yield of HCHO from isoprene (Marais et al., 2012). We advocate considering the NO_x dependence of background HCHO as well, since this can constitute a significant fraction of the total HCHO column. For scale, the derived background HCHO mixing ratio of 1.6 – 3.3 ppbv is 37 – 77% of the campaign-mean observed HCHO mixing ratio of 4.3 ppbv. Forthcoming geostationary observations will deliver sufficient resolution to delineate local gradients in chemical regime, and smearing and background HCHO production will become problematic even in high-NO_x regions. Indeed, even current-generation orbital instruments are capable of resolving urban-rural gradients in HCHO columns (Boeke et al., 2011). When applying advanced statistical techniques like inversion, model results will only be as accurate as the chemical mechanisms driving them. Continued field observations are crucial for providing confidence in our ability to link HCHO to its sources.

Acknowledgements

We are grateful to NOAA AOC and the flight crew of the WP-3D for enabling a super awesome mission. HCHO measurement efforts were supported by US EPA Science to Achieve Results (STAR) program grant 83540601 and NASA grant NNH10ZDA001N-SEAC4RS. Analysis was supported by NASA ACCDAM grant NNX14AP48G. J. Kaiser acknowledges support from NASA ESSF grant NNX14AK97H. C.D. Hatch was supported by the Hendrix faculty grant and the Hendrix College Odyssey program. This research has not been subjected to any EPA review and therefore does not necessarily reflect the views of the agency, and no official endorsement should be inferred.

441

442 **References**

443 Abbot, D. S., Palmer, P. I., Martin, R. V., Chance, K. V., Jacob, D. J., and Guenther, A.: Seasonal and
444 interannual variability of North American isoprene emissions as determined by formaldehyde
445 column measurements from space, Geophys. Res. Lett., 30, 2003.
446 Atkinson, R. and Arey, J.: Gas-phase tropospheric chemistry of biogenic volatile organic compounds: a
447 review, Atmos. Env., 37, S197 - S219, 2003.
448 Atkinson, R., Baulch, D., Cox, R., Crowley, J., Hampson, R., Hynes, R., Jenkin, M., Rossi, M., and Troe, J.:
449 Evaluated kinetic and photochemical data for atmospheric chemistry: Volume II - gas phase
450 reactions of organic species, Atmos. Chem. Phys., 6, 3625-4055, 2006.
451 Barkley, M. P., De Smedt, I., Van Roozendael, M., Kurosu, T. P., Chance, K., Arneth, A., Hagberg, D.,
452 Guenther, A., Paulot, F., Marais, E., and Mao, J. Q.: Top-down isoprene emissions over tropical South
453 America inferred from SCIAMACHY and OMI formaldehyde columns, J. Geophys. Res. Atmos., 118,
454 6849-6868, 2013.
455 Barkley, M. P., Palmer, P. I., Kuhn, U., Kesselmeier, J., Chance, K., Kurosu, T. P., Martin, R. V., Helmig, D.,
456 and Guenther, A.: Net ecosystem fluxes of isoprene over tropical South America inferred from
457 Global Ozone Monitoring Experiment (GOME) observations of HCHO columns, Journal Geophysical
458 Research, 113, D20304, 2008.
459 Boeke, N. L., Marshall, J. D., Alvarez, S., Chance, K. V., Fried, A., Kurosu, T. P., Rappengluck, B., Richter,
460 D., Walega, J., Weibring, P., and Millet, D. B.: Formaldehyde columns from the Ozone Monitoring
461 Instrument: Urban versus background levels and evaluation using aircraft data and a global model, J.
462 Geophys. Res. Atmos., 116, 2011.
463 Carlton, A. and Baker, K.: Photochemical Modeling of the Ozark Isoprene Volcano: MEGAN, BEIS, and
464 Their Impacts on Air Quality Predictions, Env. Sci. Technol., 45, 4438-4445, 2011.
465 Cazorla, M., Wolfe, G. M., Bailey, S. A., Swanson, A. K., Arkinson, H. L., and Hanisco, T. F.: A new airborne
466 laser-induced fluorescence instrument for in situ detection of Formaldehyde throughout the
467 troposphere and lower stratosphere, Atmos. Meas. Tech., 8, 541-552, 2015.
468 Crounse, J. D., Knap, H. C., Ørnsø, K. B., Jørgensen, S., Paulot, F., Kjaergaard, H. G., and Wennberg, P. O.:
469 On the atmospheric fate of methacrolein: 1. Peroxy radical isomerization following addition of OH
470 and O2, J. Phys. Chem. A, 116, 5756-5762, 2012.
471 Crounse, J. D., Paulot, F., Kjaergaard, H. G., and Wennberg, P. O.: Peroxy radical isomerization in the
472 oxidation of isoprene, Phys. Chem. Chem. Phys., 13, 13607-13613, 2011.
473 Curci, G., Palmer, P. I., Kurosu, T. P., Chance, K., and Visconti, G.: Estimating European volatile organic
474 compound emissions using satellite observations offormaldehyde from the Ozone Monitoring
475 Instrument, Atmos. Chem. Phys., 10, 11501-11517, 2010.
476 da Silva, G., Graham, C., and Wang, Z. F.: Unimolecular beta-Hydroxyperoxy Radical Decomposition with
477 OH Recycling in the Photochemical Oxidation of Isoprene, Env. Sci. Technol., 44, 250-256, 2010.
478 de Gouw, J. and Warneke, C.: Measurements of volatile organic compounds in the earths atmosphere
479 using proton-transfer-reaction mass spectrometry, Mass Spec. Rev., 26, 223-257, 2007.
480 de Gouw, J. A., McKeen, S. A., Aikin, K. C., Brock, C. A., Brown, S. S., Gilman, J. B., Graus, M., Hanisco, T.,
481 Holloway, J. S., Kaiser, J., Keutsch, F. N., Lerner, B. M., Liao, J., Markovic, M. Z., Middlebrook, A. M.,
482 Min, K. E., Neuman, J. A., Nowak, J. B., Peischl, J., Pollack, I. B., Roberts, J. M., Ryerson, T. B., Trainer,
483 M., Veres, P. R., Warneke, C., Welti, A., and Wolfe, G. M.: Airborne Measurements of the
484 Atmospheric Emissions from a Fuel Ethanol Refinery, J. Geophys. Res. Atmos., 120, 4385-4397, 2015.

de Gouw, J. A., Middlebrook, A. M., Warneke, C., Goldan, P. D., Kuster, W. C., Roberts, J. M., Fehsenfeld, F. C., Worsnop, D. R., Canagaratna, M. R., Pszenny, A. A. P., Keene, W. C., Marchewka, M., Bertman, S. B., and Bates, T. S.: Budget of organic carbon in a polluted atmosphere: Results from the New England Air Quality Study in 2002, J. Geophys. Res., 110, 2005.

DiGangi, J. P., Boyle, E. S., Karl, T., Harley, P., Turnipseed, A., Kim, S., Cantrell, C., Maudlin Iii, R. L., Zheng, W., Flocke, F., Hall, S. R., Ullmann, K., Nakashima, Y., Paul, J. B., Wolfe, G. M., Desai, A. R., Kajii, Y., Guenther, A., and Keutsch, F. N.: First direct measurements of formaldehyde flux via eddy covariance: implications for missing in-canopy formaldehyde sources, Atmos. Chem. Phys., 11, 10565-10578, 2011.

Donner, L. J., Wyman, B. L., Hemler, R. S., Horowitz, L. W., Ming, Y., Zhao, M., Golaz, J.-C., Ginoux, P., Lin, S. J., Schwarzkopf, M. D., Austin, J., Alaka, G., Cooke, W. F., Delworth, T. L., Freidenreich, S. M., Gordon, C. T., Griffies, S. M., Held, I. M., Hurlin, W. J., Klein, S. A., Knutson, T. R., Langenhorst, A. R., Lee, H.-C., Lin, Y., Magi, B. I., Malyshev, S. L., Milly, P. C. D., Naik, V., Nath, M. J., Pincus, R., Ploshay, J. J., Ramaswamy, V., Seman, C. J., Shevliakova, E., Sirutis, J. J., Stern, W. F., Stouffer, R. J., Wilson, R. J., Winton, M., Wittenberg, A. T., and Zeng, F.: The Dynamical Core, Physical Parameterizations, and Basic Simulation Characteristics of the Atmospheric Component AM3 of the GFDL Global Coupled Model CM3, Journal of Climate, 24, 3484-3519, 2011.

Dufour, G., Wittrock, F., Camredon, M., Beekmann, M., Richter, A., Aumont, B., and Burrows, J. P.: SCIAMACHY formaldehyde observations: constraint for isoprene emission estimates over Europe?, Atmos. Chem. Phys., 9, 1647-1664, 2009.

Fares, S., Paoletti, E., Loreto, F., and Brilli, F.: Bidirectional Flux of Methyl Vinyl Ketone and Methacrolein in Trees with Different Isoprenoid Emission under Realistic Ambient Concentrations, Environ Sci Technol, 49, 7735-7742, 2015.

Fortems-Cheiney, A., Chevallier, F., Pison, I., Bousquet, P., Saunois, M., Szopa, S., Cressot, C., Kurosu, T. P., Chance, K., and Fried, A.: The formaldehyde budget as seen by a global-scale multi-constraint and multi-species inversion system, Atmos. Chem. Phys., 12, 6699-6721, 2012.

Fu, T. M., Jacob, D. J., Palmer, P. I., Chance, K., Wang, Y. X. X., Barletta, B., Blake, D. R., Stanton, J. C., and Pilling, M. J.: Space-based formaldehyde measurements as constraints on volatile organic compound emissions in east and south Asia and implications for ozone, J. Geophys. Res. Atmos., 112, 2007.

Fuchs, H., Hofzumahaus, A., Rohrer, F., Bohn, B., Brauers, T., Dorn, H., Haseler, R., Holland, F., Kaminski, M., Li, X., Lu, K., Nehr, S., Tillmann, R., Wegener, R., and Wahner, A.: Experimental evidence for efficient hydroxyl radical regeneration in isoprene oxidation, Nature Geosci., 6, 1023-1026, 2013.

Guenther, A. B., Jiang, X., Heald, C. L., Sakulyanontvittaya, T., Duhl, T., Emmons, L. K., and Wang, X.: The Model of Emissions of Gases and Aerosols from Nature version 2.1 (MEGAN2.1): an extended and updated framework for modeling biogenic emissions, Geosci. Mod. Dev., 5, 1471-1492, 2012.

Hogrefe, C., Isukapalli, S. S., Tang, X. G., Georgopoulos, P. G., He, S., Zalewsky, E. E., Hao, W., Ku, J. Y., Key, T., and Sistla, G.: Impact of Biogenic Emission Uncertainties on the Simulated Response of Ozone and Fine Particulate Matter to Anthropogenic Emission Reductions, J. Air Waste Man. Assoc., 61, 92-108, 2011.

Jenkin, M. E., Young, J. C., and Rickard, A. R.: The MCM v3.3 degradation scheme for isoprene, Atmos. Chem. Phys. Discuss., 15, 9709-9766, 2015.

Kaiser, J., Wolfe, G. M., Bohn, B., Broch, S., Fuchs, H., Ganzeveld, L. N., Gomm, S., Haseler, R., Hofzumahaus, A., Holland, F., Jager, J., Li, X., Lohse, I., Lu, K., Prevot, A. S. H., Rohrer, F., Wegener, R., Wolf, R., Mentel, T. F., Kiendler-Scharr, A., Wahner, A., and Keutsch, F. N.: Evidence for an unidentified non-photochemical ground-level source of formaldehyde in the Po Valley with potential implications for ozone production, Atmos. Chem. Phys., 15, 1289-1298, 2015a.

Kaiser, J., Wolfe, G. M., Min, K. E., Brown, S. S., Miller, C. C., Jacob, D. J., deGouw, J. A., Graus, M., Hanisco, T. F., Holloway, J., Peischl, J., Pollack, I. B., Ryerson, T. B., Warneke, C., Washenfelder, R. A.,

and Keutsch, F. N.: Reassessing the ratio of glyoxal to formaldehyde as an indicator of hydrocarbon precursor speciation, Atmos. Chem. Phys., 15, 7571-7583, 2015b.
Karl, T., Harley, P., Emmons, L., Thornton, B., Guenther, A., Basu, C., Turnipseed, A., and Jardine, K.: Efficient Atmospheric Cleansing of Oxidized Organic Trace Gases by Vegetation, Science, 330, 816 - 819, 2010.
Kefauver, S. C., Filella, I., and Peñuelas, J.: Remote sensing of atmospheric biogenic volatile organic compounds (BVOCs) via satellite-based formaldehyde vertical column assessments, International Journal of Remote Sensing, 35, 7519-7542, 2014.
Kim, S., Kim, S. Y., Lee, M., Shim, H., Wolfe, G. M., Guenther, A. B., He, A., Hong, Y., and Han, J.: Impact of isoprene and HONO chemistry on ozone and OVOC formation in a semirural South Korean forest, Atmos. Chem. Phys., 15, 4357-4371, 2015.
Kim, S., Wolfe, G. M., Mauldin, L., Cantrell, C., Guenther, A., Karl, T., Turnipseed, A., Greenberg, J., Hall, S. R., Ullmann, K., Apel, E., Hornbrook, R., Kajii, Y., Nakashima, Y., Keutsch, F. N., DiGangi, J. P., Henry, S. B., Kaser, L., Schnitzhofer, R., Graus, M., Hansel, A., Zheng, W., and Flocke, F. F.: Evaluation of HOx sources and cycling using measurement-constrained model calculations in a 2-methyl-3-butene-2-ol (MBO) and monoterpene (MT) dominated ecosystem, Atmos. Chem. Phys., 13, 2031-2044, 2013.
Knighton, W. B., Herndon, S. C., Franklin, J. F., Wood, E. C., Wormhoudt, J., Brooks, W., Fortner, E. C., and Allen, D. T.: Direct measurement of volatile organic compound emissions from industrial flares using real-time online techniques: Proton Transfer Reaction Mass Spectrometry and Tunable Infrared Laser Differential Absorption Spectroscopy, Industrial & Engineering Chemistry Research, 51, 12674-12684, 2012.
Lee, M., Heikes, B. G., Jacob, D. J., Sachse, G., and Anderson, B.: Hydrogen peroxide, organic hydroperoxide, and formaldehyde as primary pollutants from biomass burning, J. Geophys. Res. Atmos., 102, 1301-1309, 1997.
Li, J., Mao, J., Min, K. E., Washenfelder, R. A., Brown, S. S., Kaiser, J., Keutsch, F. N., Wolfe, G. M., Hanisco, T. F., Pollack, I. B., Ryerson, T. B., Graus, M., Gilman, J. B., Lerner, B. M., Warneke, C., de Gouw, J. A., Brock, C. A., Middlebrook, A. M., Henderson, B. H., Naik, V., Paulot, F., and Horowitz, L. W.: Observational constraints on glyoxal production from isoprene oxidation and its contribution to organic aerosol over the Southeast United States, in preparation, 2015. 2015.
Liu, Y. J., Herdlinger-Blatt, I., McKinney, K. A., and Martin, S. T.: Production of methyl vinyl ketone and methacrolein via the hydroperoxyl pathway of isoprene oxidation, Atmos. Chem. Phys., 13, 5715-5730, 2013.
Luecken, D. J., Hutzell, W. T., Strum, M. L., and Pouliot, G. A.: Regional sources of atmospheric formaldehyde and acetaldehyde, and implications for atmospheric modeling, Atmos. Env., 47, 477-490, 2012.
Mao, J., Horowitz, L. W., Naik, V., Fan, S., Liu, J., and Fiore, A. M.: Sensitivity of tropospheric oxidants to biomass burning emissions: implications for radiative forcing, Geophys. Res. Lett., 40, 1241-1246, 2013.
Mao, J., Ren, X., Brune, W. H., Van Duin, D. M., Cohen, R. C., Park, J. H., Goldstein, A. H., Paulot, F., Beaver, M. R., Crounse, J. D., Wennberg, P. O., DiGangi, J. P., Henry, S. B., Keutsch, F. N., Park, C., Schade, G. W., Wolfe, G. M., and Thornton, J. A.: Insights into hydroxyl measurements and atmospheric oxidation in a California forest, Atmos. Chem. Phys., 12, 8009-8020, 2012.
Marais, E. A., Jacob, D. J., Kurosu, T. P., Chance, K., Murphy, J. G., Reeves, C., Mills, G., Casadio, S., Millet, D. B., Barkley, M. P., Paulot, F., and Mao, J.: Isoprene emissions in Africa inferred from OMI observations of formaldehyde columns, Atmos. Chem. Phys., 12, 6219-6235, 2012.

579 Marvin, M., Wolfe, G. M., Salawitch, R., and Coworkers: Evaluating mechanisms for isoprene oxidation
580 using a constrained chemical box model and SENEX observations of formaldehyde, in preparation,
581 2015. 2015.
582 McNeill, V. F., Woo, J. L., Kim, D. D., Schwier, A. N., Wannell, N. J., Sumner, A. J., and Barakat, J. M.:
583 Aqueous-Phase Secondary Organic Aerosol and Organosulfate Formation in Atmospheric Aerosols: A
584 Modeling Study, Env. Sci. Technol., 46, 8075-8081, 2012.
585 Millet, D. B., Jacob, D. J., Boersma, K. F., Fu, T. M., Kurosu, T. P., Chance, K., Heald, C. L., and Guenther,
586 A.: Spatial distribution of isoprene emissions from North America derived from formaldehyde
587 column measurements by the OMI satellite sensor, J. Geophys. Res. Atmos., 113, 2008.
588 Millet, D. B., Jacob, D. J., Turquety, S., Hudman, R. C., Wu, S. L., Fried, A., Walega, J., Heikes, B. G., Blake,
589 D. R., Singh, H. B., Anderson, B. E., and Clarke, A. D.: Formaldehyde distribution over North America:
590 Implications for satellite retrievals of formaldehyde columns and isoprene emission, J. Geophys. Res.
591 Atmos., 111, 2006.
592 Naik, V., Horowitz, L. W., Fiore, A. M., Ginoux, P., Mao, J., Aghedo, A. M., and Levy, H., II: Impact of
593 preindustrial to present-day changes in short-lived pollutant emissions on atmospheric composition
594 and climate forcing, J. Geophys. Res. Atmos., 118, 8086-8110, 2013.
595 Palmer, P. I., Abbot, D. S., Fu, T. M., Jacob, D. J., Chance, K., Kurosu, T. P., Guenther, A., Wiedinmyer, C.,
596 Stanton, J. C., Pilling, M. J., Pressley, S. N., Lamb, B., and Sumner, A. L.: Quantifying the seasonal and
597 interannual variability of North American isoprene emissions using satellite observations of the
598 formaldehyde column, J. Geophys. Res. Atmos., 111, 2006.
599 Palmer, P. I., Jacob, D. J., Fiore, A. M., Martin, R. V., Chance, K., and Kurosu, T. P.: Mapping isoprene
600 emissions over North America using formaldehyde column observations from space, J. Geophys.
601 Res. Atmos., 108, 2003.
602 Paulot, F., Crounse, J. D., Kjaergaard, H. G., Kroll, J. H., Seinfeld, J. H., and Wennberg, P. O.: Isoprene
603 photooxidation: new insights into the production of acids and organic nitrates, Atmos. Chem. Phys.,
604 9, 1479-1501, 2009a.
605 Paulot, F., Crounse, J. D., Kjaergaard, H. G., Kurten, A., St Clair, J. M., Seinfeld, J. H., and Wennberg, P. O.:
606 Unexpected Epoxide Formation in the Gas-Phase Photooxidation of Isoprene, Science, 325, 730-733,
607 2009b.
608 Peeters, J., Muller, J.-F., Stavrakou, T., and Nguyen, V. S.: Hydroxyl Radical Recycling in Isoprene
609 Oxidation Driven by Hydrogen Bonding and Hydrogen Tunneling: The Upgraded LIM1 Mechanism, J.
610 Phys. Chem. A, 118, 8625-8643, 2014.
611 Peeters, J. and Müller, J. F.: HOx radical regeneration in isoprene oxidation via peroxy radical
612 isomerisations. II: experimental evidence and global impact, Phys. Chem. Chem. Phys., 12, 14227-
613 14235, 2010.
614 Peeters, J., Nguyen, T. L., and Vereecken, L.: HOx radical regeneration in the oxidation of isoprene, Phys.
615 Chem. Chem. Phys., 11, 5935-5939, 2009.
616 Peeters, J., Vandenberk, S., Piessens, E., and Pultau, V.: H-atom abstraction in reactions of cyclic
617 polyalkenes with OH, Chemosphere, 38, 1189-1195, 1999.
618 Pollack, I., Lerner, B., and Ryerson, T.: Evaluation of ultraviolet light-emitting diodes for detection of
619 atmospheric NO2 by photolysis - chemiluminescence, J. Atmos. Chem., 65, 111-125, 2010.
620 Rivera-Rios, J. C., Nguyen, T. B., Crounse, J. D., Jud, W., St Clair, J. M., Mikoviny, T., Gilman, J. B., Lerner,
621 B. M., Kaiser, J. B., de Gouw, J., Wisthaler, A., Hansel, A., Wennberg, P. O., Seinfeld, J. H., and
622 Keutsch, F. N.: Conversion of hydroperoxides to carbonyls in field and laboratory instrumentation:
623 Observational bias in diagnosing pristine versus anthropogenically controlled atmospheric
624 chemistry, Geophys. Res. Lett., 41, 8645-8651, 2014.
625 Roberts, J. M., Marchewka, M., Bertman, S. B., Goldan, P., Kuster, W., de Gouw, J., Warneke, C.,
626 Williams, E., Lerner, B., Murphy, P., Apel, E., and Fehsenfeld, F. C.: Analysis of the isoprene chemistry

observed during the New England Air Quality Study (NEAQS) 2002 intensive experiment, J. Geophys. Res., 111, 2006.
Ryerson, T., Huey, L., Knapp, K., Neuman, J., Parrish, D., Sueper, D., and Fehsenfeld, F.: Design and initial characterization of an inlet for gas-phase NOy measurements from aircraft, J. Geophys. Res. Atmos., 104, 5483-5492, 1999.
Shim, C., Wang, Y., Choi, Y., Palmer, P. I., Abbot, D. S., and Chance, K.: Constraining global isoprene emissions with Global Ozone Monitoring Experiment (GOME) formaldehyde column measurements, J. Geophys. Res., 110, 2005.
Stavrakou, T., Müller, J.-F., de Smedt, I., Van Roozendael, M., van der Werf, G. R., Giglio, L., and Guenther, A.: Evaluating the performance of pyrogenic and biogenic emission inventories against one decade of space-based formaldehyde columns, Atmos. Chem. Phys., 9, 1037-1060, 2009.
Stavrakou, T., Müller, J. F., Bauwens, M., De Smedt, I., Van Roozendael, M., Guenther, A., Wild, M., and Xia, X.: Isoprene emissions over Asia 1979-2012: impact of climate and land-use changes, Atmos. Chem. Phys., 14, 4587-4605, 2014.
Stroud, C., Roberts, J., Goldan, P., Kuster, W., Murphy, P., Williams, E., Hereid, D., Parrish, D., Sueper, D., Trainer, M., Fehsenfeld, F., Apel, E., Riemer, D., Wert, B., Henry, B., Fried, A., Martinez-Harder, M., Harder, H., Brune, W., Li, G., Xie, H., and Young, V.: Isoprene and its oxidation products, methacrolein and methylvinyl ketone, at an urban forested site during the 1999 Southern Oxidants Study, J. Geophys. Res. Atmos., 106, 8035-8046, 2001.
Trainer, M., Williams, E., Parrish, D., Buhr, M., Allwine, E., Westberg, H., Fehsenfeld, F., and Liu, S.: Models and observations of the impact of natural hydrocarbons on rural ozone, Nature, 329, 705-707, 1987.
Wagner, N. L., Brock, C. A., Angevine, W. M., Beyersdorf, A., Campuzano-Jost, P., Day, D., de Gouw, J. A., Diskin, G. S., Gordon, T. D., Graus, M. G., Holloway, J. S., Huey, G., Jimenez, J. L., Lack, D. A., Liao, J., Liu, X., Markovic, M. Z., Middlebrook, A. M., Mikoviny, T., Peischl, J., Perring, A. E., Richardson, M. S., Ryerson, T. B., Schwarz, J. P., Warneke, C., Welti, A., Wisthaler, A., Ziemba, L. D., and Murphy, D. M.: In situ vertical profiles of aerosol extinction, mass, and composition over the southeast United States during SENEX and SEAC⁴RS: observations of a modest aerosol enhancement aloft, Atmos. Chem. Phys., 15, 7085-7102, 2015.
Warneke, C., de Gouw, J. A., Del Negro, L., Brioude, J., McKeen, S., Stark, H., Kuster, W. C., Goldan, P. D., Trainer, M., Fehsenfeld, F. C., Wiedinmyer, C., Guenther, A. B., Hansel, A., Wisthaler, A., Atlas, E., Holloway, J. S., Ryerson, T. B., Peischl, J., Huey, L. G., and Hanks, A. T. C.: Biogenic emission measurement and inventories determination of biogenic emissions in the eastern United States and Texas and comparison with biogenic emission inventories, J. Geophys. Res. Atmos., 115, 21, 2010.
Wolfe, G. M., Cantrell, C., Kim, S., Mauldin III, R. L., Karl, T., Harley, P., Turnipseed, A., Zheng, W., Flocke, F., Apel, E. C., Hornbrook, R. S., Hall, S. R., Ullmann, K., Henrey, S. B., DiGangi, J. P., Boyle, E. S., Kaser, L., Schnitzhofer, R., Hansel, A., Graus, M., Nakashima, Y., Kajii, Y., Guenther, A., and Keutsch, F. N.: Missing peroxy radical sources within a summertime ponderosa pine forest, Atmos. Chem. Phys., 14, 4715-4732, 2014.
Wolfe, G. M., Crounse, J. D., Parrish, J. D., St. Clair, J. M., Beaver, M. R., Paulot, F., Yoon, T. P., Wennberg, P. O., and Keutsch, F. N.: Photolysis, OH reactivity and ozone reactivity of a proxy for isoprene-derived hydroperoxyenals (HPALDs), Phys. Chem. Chem. Phys., 14, 7276-7286, 2012.
Xu, L., Guo, H., Boyd, C. M., Klein, M., Bougiatioti, A., Cerully, K. M., Hite, J. R., Isaacman-VanWertz, G., Kreisberg, N. M., Knote, C., Olson, K., Koss, A., Goldstein, A. H., Hering, S. V., de Gouw, J., Baumann, K., Lee, S.-H., Nenes, A., Weber, R. J., and Ng, N. L.: Effects of anthropogenic emissions on aerosol formation from isoprene and monoterpenes in the southeastern United States, P. Nat. Acad. Sci. USA, 112, 37-42, 2015.

674

675

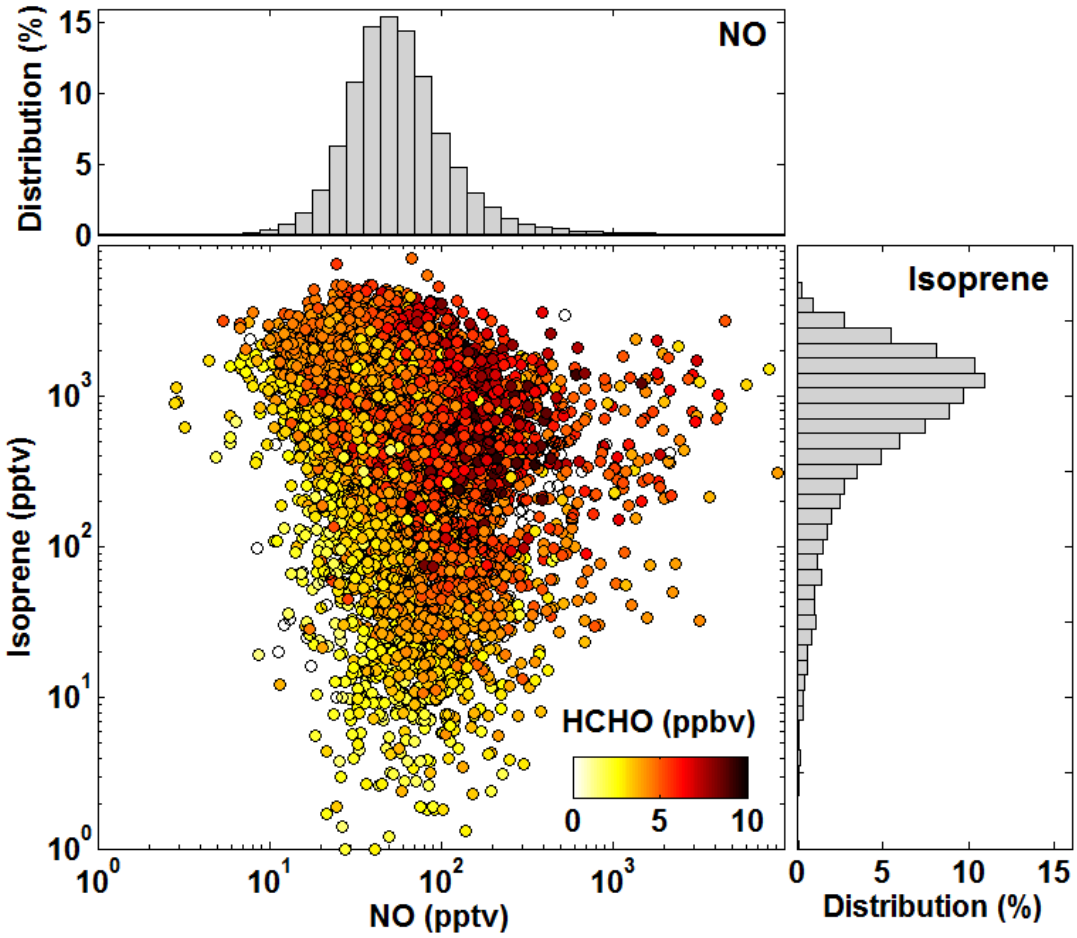

676

677 **Figure 1.** Co-variation of isoprene, NO and HCHO mixing ratios in the summertime southeast U.S. Data
678 are limited to daytime boundary layer observations. Histograms show the sampled NO and isoprene
679 distributions.

680

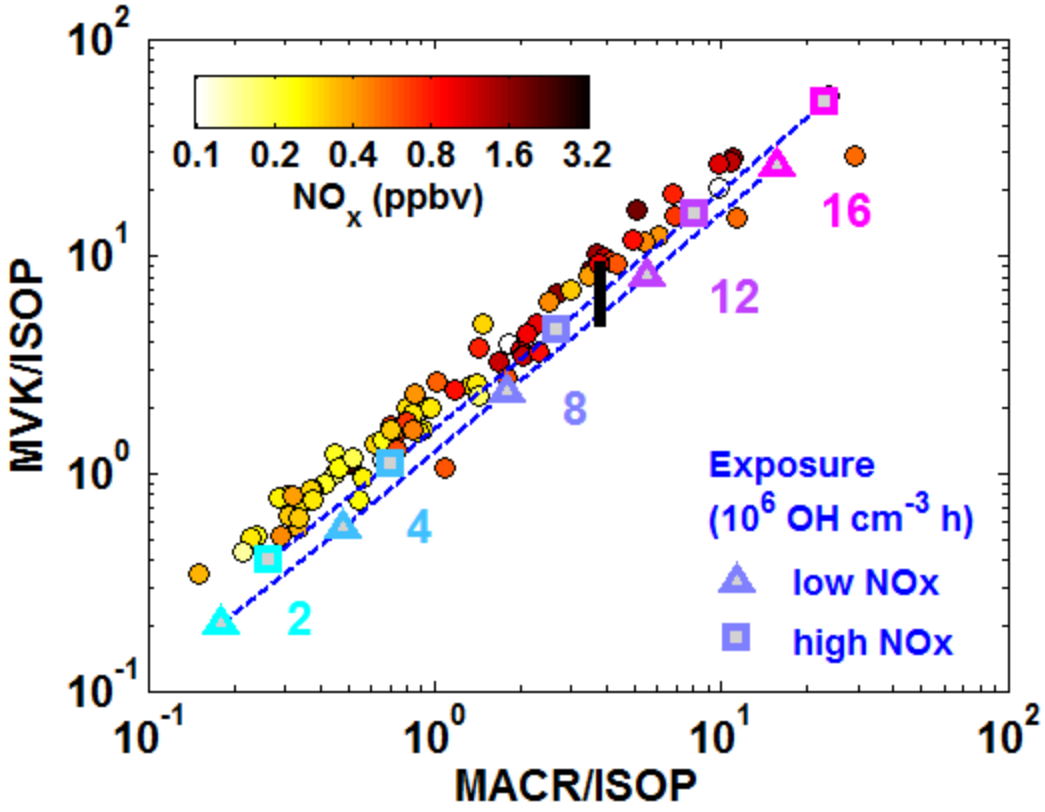

681

682 **Figure 2.** A photochemical clock of isoprene oxidation defined by the progression of daughter/parent
683 ratios. Solid circles show the observed ratios calculated from iWAS observations, colored by NO_x.
684 Blue/purple symbols, dashed lines, and text indicate the theoretical exposures (the product of OH
685 concentration and time) corresponding to any given daughter/parent relationship. Theoretical values
686 are calculated at 298K using MVK and MACR yields for NO values of 50 pptv (triangles) and 1000 pptv
687 (squares). The thick black line denotes the systematic error due to a potential 50% positive artifact in
688 MVK observations (see SI).

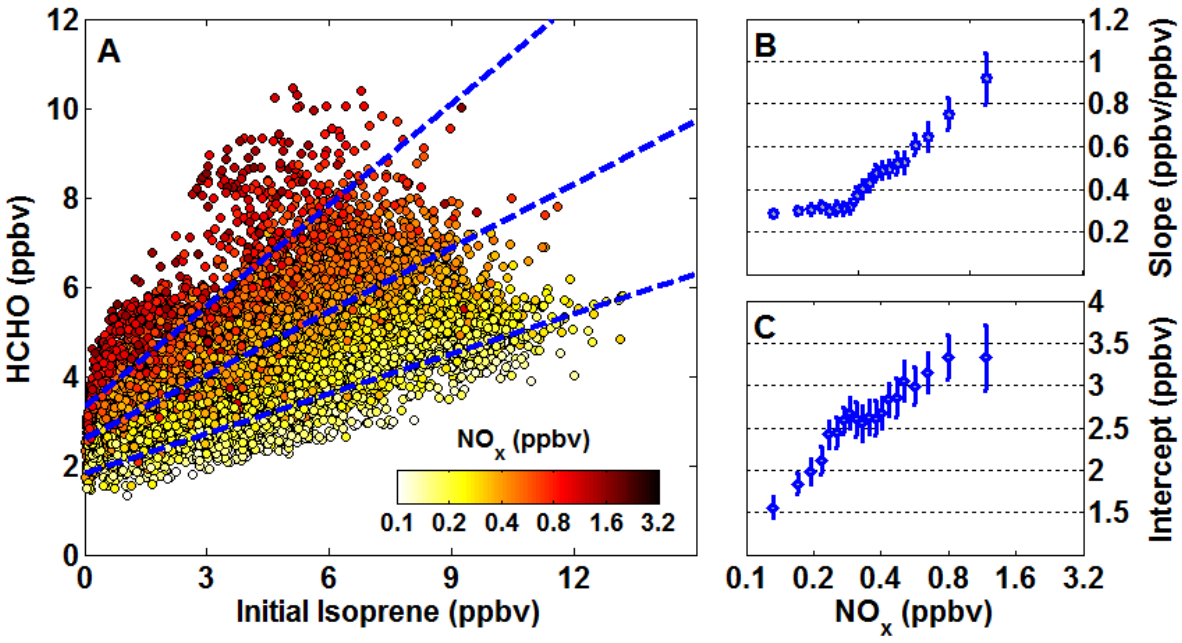

689

690 **Figure 3.** (A) NO_x modulates the relationship between observed HCHO and calculated initial isoprene
691 mixing ratios. Symbols denote all 1-second data points. Dashed lines illustrate representative major-axis
692 fits of NO_x-grouped subsets at mean NO_x values of 170, 380 and 810 pptv (see text for details of fitting
693 procedure). The slope (B) and intercept (C) of these fits are the prompt HCHO yield and background
694 HCHO mixing ratio, respectively. Error bars in (B) and (C) are 3σ fitting uncertainties.

695

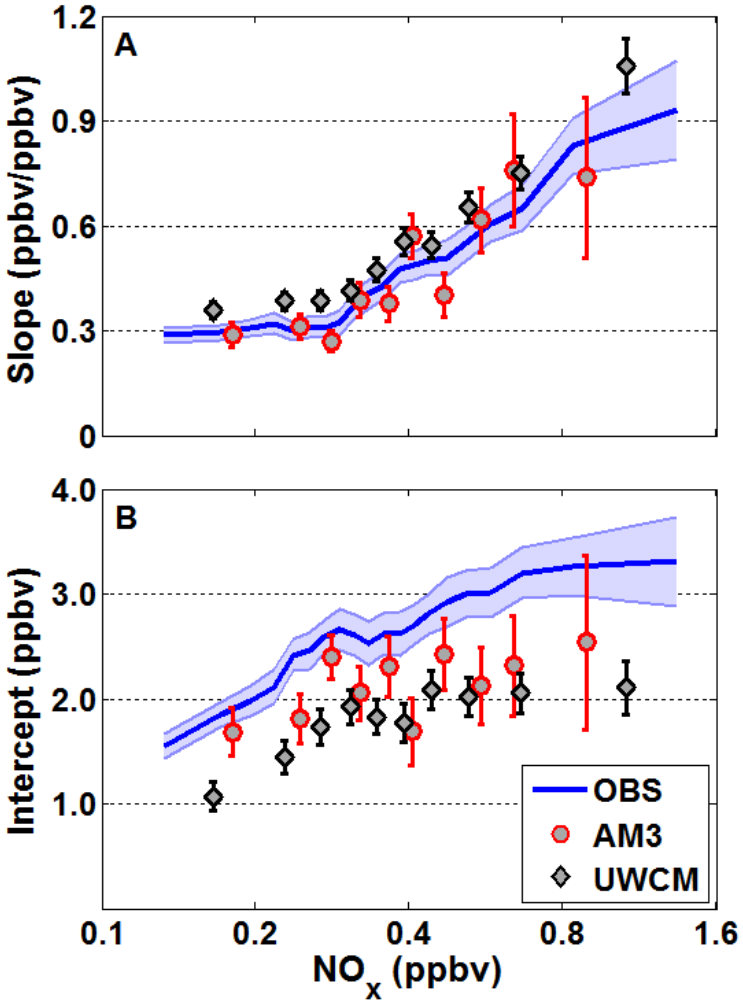

696

697 **Figure 4.** Comparison of observed and model-derived relationship between HCHO and initial isoprene
698 versus NO_x. Slopes (A) and intercepts (B) are calculated as described in the text. The observed values
699 (blue line with shading) are the same as those shown in Figs. 3B-C. Symbols represent fit results for the
700 global AM3 model (red circles) and the 0-D UWCM box model (black diamonds). Error bars denote 3σ
701 fitting uncertainties.

702

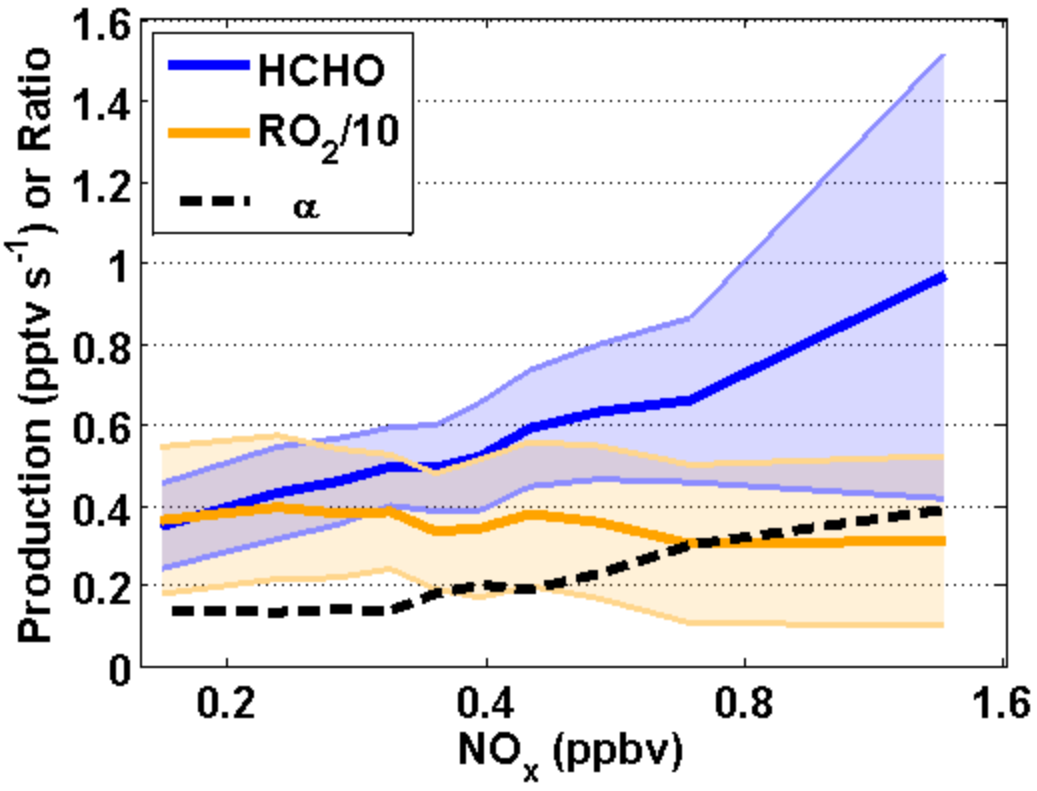

703

704 **Figure 5.** NO_x dependence of chemical properties related to HCHO production, extracted from the
705 UWCM simulation of SENEX observations. Production rates for HCHO (blue) and total RO_2 (orange) are
706 averaged over NO_x using 10 bins with equal numbers of points. Solid lines show the mean, shading is 1σ
707 variability. Note that RO_2 production is scaled down by a factor of 10. The ratio of HCHO to RO_2
708 production gives the bulk HCHO branching ratio (dashed line).